

Solid-State Characterization of Heteropolyacid-Phyllosilicate Complexes: Structural, Morphological and Thermal Properties

Pascal Y. Vuillaume¹, Asmae Mokrini², Lucie Robitaille², Philippe Bébin¹ & Lori Leblond¹

¹ COALIA, 671 Blvd. Frontenac West, Thetford Mines, Qc, G6G 1N1 Canada

² National Research Council Canada, Industrial Materials Institute, Boucherville, Qc, J4B 6Y4 Canada

Correspondence: Pascal Vuillaume, COALIA, 671, Bould. Frontenac West, Thetford Mines, Qc, G6G 1N1 Canada.
Tel: 1-418-814-8264. E-mail: pvuillaume@coalia.ca

Received: April 16, 2023

Accepted: May 16, 2023

Online Published: May 23, 2023

doi:10.5539/jmsr.v12n1p36

URL: <https://doi.org/10.5539/jmsr.v12n1p36>

Abstract

We have previously described the complex formation from a synthetic smectite clay, Sumecton SA (SSA), and the heteropolyacid (HPA), 12-phosphotungstic acid (PTA). Three new synthetic layered aluminosilicate clays of the smectite- [Lucentite SWN (SWN)] and (fluoro)mica-type [Tetrasilicic mica (TSM); Somasif ME100, (SME)] have been self-assembled with PTA, at a specific PTA-clay weight ratio of 5. New protogenic inorganic complexes have been prepared for the future fabrication of proton exchange membrane for fuel cell devices (PEMFC). Complex formation, thermal and structural properties of PTA-phyllosilicate complexes have been investigated using EDX, XRD, SEM, and DRIFT. EDX indicates that complexes incorporate a substantial amount of PTA (50-60% w/w) and that a moderate depletion of Mg²⁺ ions from octahedral layers of micas clays occurs during the process compared to smectite ones. In contrast, a significant amount of F is removed from the octahedral framework of the mica clays. DRIFT experiments indicate that the Keggin structure is preserved within all complexes and that complex formation predominantly involves the external oxygen (W-O_d) of PTA. According to Patterson functions, coherence lengths - which reflect for the virgin clays the extent of the longitudinal platelet stacking (L_c) - of the two smectite clays (L_c ~25 Å) are significantly lower than for their analogous of the mica type (L_c = 180-225 Å). Clays in complexes are characterized by the loss of in-plane organization but are still partially ordered. The nature of the order is still speculative but could be related to the formation of a new inorganic PTA species formed during the complex formation. Compared to the virgin clays, the order of smectite complexes is maintained in the same range (L_c = 27-42 Å) while for mica complexes, coherence lengths are dramatically reduced to ~ 60 Å. All PTA-activated complexes contain a substantial amount of amorphous silica, which tends to increase when heated at temperatures above 280 °C. However, the Keggin structure within the complexes is at least stable up to 280 °C and even, for the most robust TSM complex, up to 450 °C.

Keywords: Clays, heteropolyacids, protogenic complexes, Patterson functions, coherence length

1. Introduction

Phyllosilicates clays are layered self-assemblies built-up from silicate (Si-O) nanoplates. Within this class of inorganic materials are found the swelling smectite- and mica-type clays. Both have a similar structural edifice (see Figure 1); the distinction between the two groups is based on the surface charge density and elemental composition. Micas are characterized by a higher negative charge density (~1 per formula unit cell layer) than smectite (~0.2 to 0.6). (Note 1) Because of their low cost, availability and unusual intercalation properties, a large variety of natural swelling smectite and micas clays has been used for forming new functional materials (Sanchez, Julian, Belleville, & Popall, 2005). Some acid activated phyllosilicates clays have been used as catalytic supports (Yadav, 2005) or for the fabrication of proton exchange membrane for fuel cell devices (PEMFC) (Herring, 2006). In the PEMFC field, there is an immediate need to design viable polyelectrolyte membrane with high protogenic conductivity capable of operating at low humidity level and/or high temperature and durability (Herring, 2006).

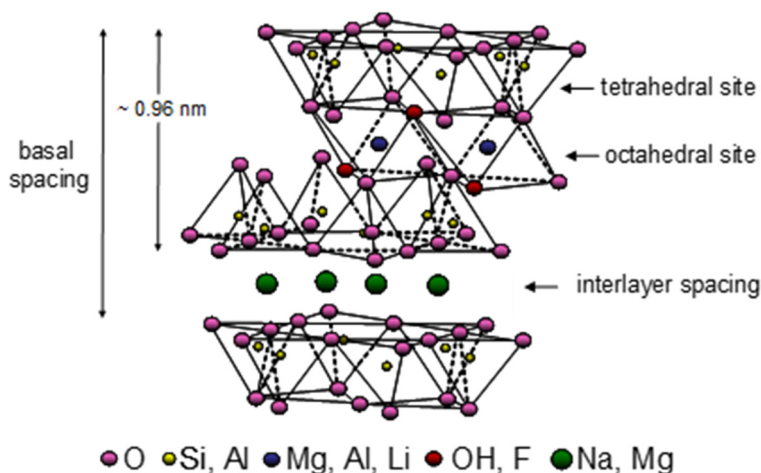


Figure 1. Schematic representation for the smectite- and mica-type structures

The immobilization through electrostatic interactions/hydrogen bonding of protogenic objects on the surface of silicate materials before being incorporated within polyelectrolyte membrane should prevent substantial leaching in a fuel cell environment. In addition, this strategy avoids the costly and time-consuming synthetic approach used to covalently bond the protogenic moieties to silicate or to any other substrate (Liu, 2007). Recently, we have shown that the 12-phosphotungstic heteropolyacid (PTA), an inorganic acid with intrinsic proton activity [$0.18 \text{ S}\cdot\text{cm}^{-1}$ in its hydrated crystalline form ($\text{H}_3\text{PW}_{12}\text{O}_{40}\cdot 29\text{H}_2\text{O}$)] (Nakamura, Kodama & Ogino, 1979), interacts with the smectite-like clay, Sumecton SA (SSA), to form robust PTA-SSA complexes (Vuillaume et al., 2009). The basic structural unit of PTA is the Keggin anion for which a schematic representation is shown in Figure 2. The polyhedral structure of PTA of Keggin type consists of a central PO_4 tetrahedron surrounded by 12 WO_6 octahedra. Octahedra are self-assembled by three, sharing common edges for forming (W_3O_{13}) tritungstic units. Four types of oxygen atoms are present in the Keggin structure. O_a atoms are oxygen connected to the PO_4 tetrahedron while O_b and O_c oxygen atoms link the tungsten atoms from two distinct W_3O_{13} units or from the same unit, respectively. The terminal oxygen, O_d , are only bonded to one tungsten atom.

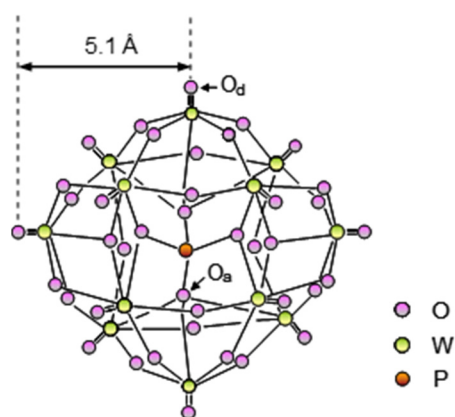


Figure 2. Schematic representation of the 12-phosphotungstic heteropolyacid Keggin structure. O_a atoms are oxygen connected to the PO_4 tetrahedron while O_d is bonded to one tungsten. O_b and O_c oxygen that link tungsten atoms are not mentioned because they cannot be distinguished adequately from this representation. Size is estimated from crystallographic data for Keggin ion salt (see ref. Spirlet & Busing, 1978)

The strong Brønsted acid PTA is known to have a notable activity on the clay structure, in particular for saponite-like clays. (Okada et al., 2007) In a previous publication (Vuillaume et al., 2009), we have demonstrated that the SSA-PTA weight ratio used for the preparation of the complexes determines, at least in part - since the temperature

and other factors for the complexation may play also an important factor (Okada et al., 2006; Linssen et al., 2002; Kooli & Jones, 1997; Okada et al., 2005; Okada et al., 2002), the degree of amorphization of the complex.

So far, functionalization of clays with heteropolyacids has been essentially restricted to smectite clays, principally montmorillonite (Yadav, 2005; Marme, Coudurier, & Vedrine, 1998) as well as layered double hydroxides (LDH) (Changween et al., 2001). In this work, we explore the possibility of forming, partially disordered PTA-containing hybrid materials, with high amount of PTA, from different phyllosilicates clay, including fluoronano clays.

It is not in our interest to induce pillaring that would result in the isolation of the PTA Keggin units from each other's. We rather try to promote a robust immobilization of the Keggin units within a silica network that would favour the PTA proximity. In the following, we describe the preparation and solid-state characterization of new low-cost clay-heteropolyacid complexes and will present a comparison of the effect of different clay type on the amorphization process leading to the formation of the nanoparticles.

To this end, we have chosen, in addition to SSA which was investigated elsewhere (Vuillaume et al., 2009), three types of synthetic 2:1 layered phyllosilicate clays, including Lucentite SWN (SWN), sodium fluorotetrasilic mica (TSM) and Somasif ME100 (SME). SSA and SWN are both smectite clays with a saponite- and a hectorite-like structure, respectively. Both have a trioctahedral structure (all octahedral sites are filled by cations). For both smectite clays, Mg^{2+} ions are located within the octahedral layer, sandwiched between two layers of tetrahedral Si^{4+} ions. For SSA, the isomorphous substitution of Al^{3+} for Si^{4+} leads to a deficit of charge in the tetrahedral layer while for SWN, the replacement of some Mg^{2+} ions by Li^{+} ions create a layer charge deficit in the octahedral layers. The negative charges within the lattice are neutralized by the absorption of Na^{+} on the silicate surface. For the two fluoro-mica used in this work (TSM and SME), octahedral layers only contain Mg^{2+} ions. However, these micas are intermediate between dioctahedral and trioctahedral, due to their incomplete occupation of their octahedral layers and thus, negative charge in the central octahedral sheet arises from Mg^{2+} vacancies. Tetrahedral sheets of TSM are pure SiO_2 sheet while for SME, few Al^{3+} ions replaced Si^{4+} ions, creating, in addition, negatively charged tetrahedral layers. TSM is similar to SME but contains less Mg^{2+} and more Na^{+} and in both mica clays, the hydroxyl groups are completely substituted by fluorine atoms.

2. Experimental

2.1 Materials

SSA [11.2% weight loss of ignition] was kindly provided by Kunimine Industries Co. and used without further purification. SSA with a theoretical ideal structural formula $[(Si_{7.20}Al_{0.80})(Mg_{5.97}Al_{0.03})O_{20}(OH)_4]^{0.77}(Na_{0.49}Mg_{0.14})^{+0.77}$ is a synthetic inorganic polymer with a saponite-like structure. SWN (Coop Chemicals) has a general molecular structure of $Na_{0.33}[(Mg_{2.67}Li_{0.33})(Si_4O_{10})(OH)_2]$. The two sodium fluorotetrasilic mica provided by TSM (Topy Ind.) and SME (Coop Chemicals) are both synthetic 2:1 layered silicates with charge density higher than that of smectite and ideal chemical formula $[NaMg_{2.5}(Si_4O_{10})F_2]$ and $[Na_{0.66}Mg_{2.68}(Si_{3.98}Al_{0.02})O_{10.02}F_{1.96}]$, respectively. Small amounts of impurities may be present in the above formulas. For example, TSM contains a small amount of Al and was purified by Topy Industries according to their own procedure. 12-phosphotungstic acid was obtained from Aldrich in pure form (99.995 %). Water used for the dispersion of the clays was purified by a Millipore Milli-Q system (resistance 18.2 M Ω).

2.2 Preparation and Characterization of Clay-Heteropolyacid Dispersions

Clays were sonicated in water (400 mL) at a concentration of 0.6 % (w/w) for 4 hours at 60 °C. The suspension was found very stable since no visible flocculation is apparent during the following day. To prepare PTA-clay complexes, the clay dispersion was added to a warm (60 °C) concentrated aqueous solution (100 ml) of PTA. To ensure high loading, high PTA-clay weight ratio was used, namely 5. The dispersion was again sonicated at 60 °C for 1 hr and, again a stable aqueous suspension was obtained. Therefore, water was rotary evaporated and the obtained white powder. The sample was further dried under vacuum at 125 °C for 1h. The complex was washed by stirring vigorously two times with 100 mL methanol for 30 min, filtered and dried overnight at 60 °C. White powder was obtained after the final washing and drying.

2.3 Energy-Dispersive X-Ray Spectroscopy (EDX)

Elemental characterization of the clays, PTA acid and complexes were performed by EDX using a Hitachi S4700 scanning electron microscope. Microanalysis was performed at three points using a voltage of 10 KeV. Absorption spectra were collected with Oxford spectrometer (Model 7200) with a detector area of 20 mm² and with a resolution of 136 eV at 5.9 KeV.

2.4 Fourier Transformed Diffuse Reflectance Spectroscopy (DRIFT)

Infrared spectra were recorded on a Nicolet Magna 860 FT-IR from Thermo Electron Corp. (DTGS detector, resolution 2 cm^{-1} , accumulation of 128 scans). Diffuse reflexion was measured with "praying Mantis" accessory from Harrick Scientific Corp. Samples were dried at $125\text{ }^{\circ}\text{C}$, grinded very finely with dried KBr, dried again under vacuum at $60\text{ }^{\circ}\text{C}$ for two hours, and finally stored under a dried nitrogen atmosphere for 2 days before recording the spectra. Diffuse reflectance spectra were converted to absorbance by the Kubelka-Munk method. The maxima were obtained after smoothing the data by the Fourier function. DRIFT experiments were also carried out for complexes previously heated for 18 h at $280\text{ }^{\circ}\text{C}$ (under dynamic vacuum), $450\text{ }^{\circ}\text{C}$ (under static vacuum) and $600\text{ }^{\circ}\text{C}$ (under air atmosphere). Complex spectra have been subtracted from the spectrum of the pristine clay spectra obtained in the same conditions to precise the position of these new vibrations' bands. Peak decomposition was performed using the GRAMS/32 software from Thermo Galactic Corp. Gaussian line shapes provided the best fit.

2.5 Scanning Electron Microscopy (SEM)

FEG-SEM Hitachi S-4700 microscope was used at low voltage for examination of the morphology of PTA and PTA-clay complexes. Clay and complexes were dried at $60\text{ }^{\circ}\text{C}$ overnight under vacuo and then were suspended by sonication for 30 min in methanol in diluted conditions (10^{-3} g/L). Drops of the dispersion were deposited on a porous polycarbonate membrane (SPI®, pore size = $0.22\text{ }\mu\text{m}$), air-dried, coated with Pt, and observed such as.

2.6 Wide Angle and Small Angle X-Ray Scattering (WAXS and SAXS)

PTA, clays, and complexes were analysed by WAXS to evaluate their structural characteristics. The diffraction patterns were first recorded on a Bruker Discover 8 diffractometer operating at 40 kV , 40 mA with $\text{Cu K}\alpha$ radiation in reflection mode using a horizontal Bragg-Brentano focusing geometry. Samples were previously dried at $60\text{ }^{\circ}\text{C}$, gently pressed for the analysis but exposed to the moisture of air during the experiment. The first set of data covered angles between 3 and 70° . Correction for the background was not performed and maxima were obtained after smoothing the data by the Savitsky Golay algorithm. The d-spacings were determined from the diffraction peaks using Bragg's relation, $d = \lambda/(2 \cdot \sin\theta)$.

SAXS experiments were carried out in transmission mode over a q range varying between 0.032 and $0.87\text{ }\text{\AA}^{-1}$ in order to use the classical approach of the one dimensional correlation function or Patterson function, $P(r)$. The SAXS intensity of the investigated material, $I(q)$, is the function of the scattering angle (2θ) and wavelength (λ) of the applied radiation. This relation can be expressed as $q = 4\pi \cdot \sin\theta/\lambda$ where q is the scattering vector. The samples under the form of dried powder ($60\text{ }^{\circ}\text{C}$ under vacuo, overnight) were placed into 1.5 mm i.d. Lindemann capillaries (Charles Supper) sealed or let open to study samples in their hydrated form (exposition to humid atmosphere condition). The diffraction patterns were recorded by a Bruker AXS two-dimensional position-sensitive wire-grid detector. The sample-to-detector distance was fixed at 10 cm and collimation was effected by a graphite monochromator and a 0.8 mm pinhole. A correction for the background was performed with empty capillaries and the curve was extrapolated to 0° to prevent any truncation in the $P(r)$. $P(r)$ functions were obtained by Fourier transformation. Bragg distances were obtained from Patterson function from the maximum of the first oscillation or, when significant oscillations were regularly spaced, from the distance separating two subsequent oscillations. Coherence lengths, L_c , were also obtained by fitting an exponential function [$\exp(-z/\zeta)$] passing through the subsidiary maxima of the Patterson functions. Coherence lengths given in Table 2 were defined as $L_c = 3\zeta$ which represents approximately the largest distance over which correlation subsides between layers.

3. Results and Discussion

The elemental composition of clay and complexes was investigated by energy dispersive X-ray spectroscopy (EDX). EDX spectra of PTA, pristine clays and complexes extensively prepared at a PTA-clay weight ratio of 5, are presented in Figure 3. Peaks observed in the EDX spectrum of PTA are identified and assigned to elements W, O and P (see Figure 2). W signals are easily noted at 1.38 , 1.79 and is a probably a part of the signal observed around 2.3 KeV .

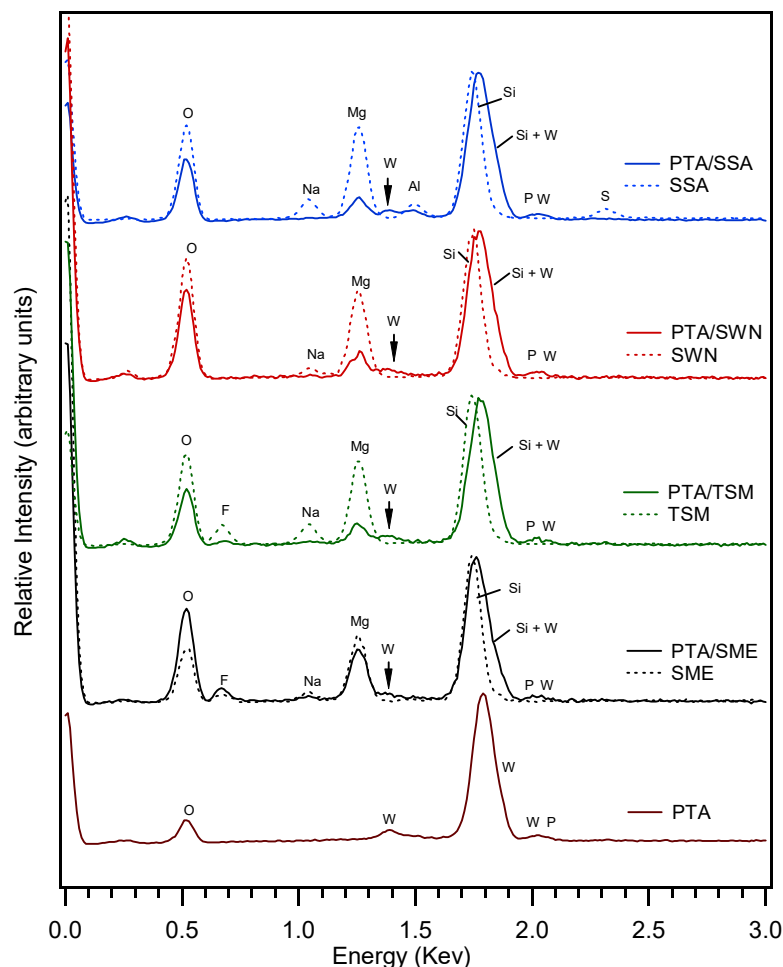


Figure 3. EDX spectra (dashed lines for the pristine clays and solid lines for the complexes) of PTA heteropolyacid (brown) and PTA-clay complexes prepared at a weight ratio of 5: SWN and PTA/SWN (red); TSM and PTA/TSM (green); SME and PTA/SME (black); SSA and PTA/SSA (blue). Spectra were normalized against the peak intensity found at 1.79 KeV. Data are displaced vertically for clarity

Peaks corresponding to O are visible at 0.52 KeV while P signal is barely seen at ~ 2.0 KeV, respectively. In the spectra of the pure clays (Figure 3. c,e,g,i), the usual distinct peaks of O, Si, Al, Mg and Na are observed at 0.52, 1.74, 1.49, 1.26 and 1.04 KeV, respectively. For the complexes, major changes are noticed. The main Si and W signals are convolved to give a broader signal whose maximum is observed at ~ 1.79 KeV. For all types of clays, the disappearance of the sodium peak at 1.04 KeV is observed, confirming that Na^+ counterions are quasi completely removed from the clay structure during the complex formation. This was also noticed for other saponites leached out with sulfuric or hydrochloric acids. Other studies have shown that upon complexation of the activated clay material with HPA, the interlayer compensating cations are exchanged for the protons of the HPA. On the other hand, for SSA, the Si/Al ratio is almost identical to that in pristine clay and for both SSA and SWN, a significant proportion of Mg ions, roughly calculated to be 25-30%, are removed from the octahedral framework, as indicated by the increase in the Si/Mg ratio (see Table 1). As noticed elsewhere for other saponite-like clays, a severe acid activation (that depends on both acid concentration and time of treatment) is needed to completely leach out the Mg^{2+} cations. In contrast with the two smectite clays, results indicate that PTA treatment is not aggressive enough to displace a large number of octahedral cations of the mica-type clay. The Si/Mg ratio of TSM and SME complexes indicates that ~ 5 and $\sim 13\%$ are displaced from their initial octahedral positions, respectively. In contrast, a rather significant amount of F seems to be leached from their tetrahedral position since the fluorine in the same proportion for TSM and SME by approximately 33%. For all complexes, a large amount of W is incorporated. For the two smectites clays, ratios Si/W are identical (0.16) while for the mica-based complexes, the ratio is much lower for TSM indicating that (0.08) is much higher than for SME (0.33).

Table 1. Elemental composition obtained from semi-quantitative EDX analysis for the heteropolyacid (PTA), the clays and their complexes (PTA-clay) formed at a weight ratio of 5. Calculated data obtained from the theoretical formula are given in parenthesis

	O	Li	Na	F	Mg	Al	Si	W	P	Si/Al	Si/W	Si/F	Si/Mg
SSA ^{a)}	45.3 (49.9)	-	3.9 (1.9)	-	16.5 (19.3)	2.6 (2.9)	29.4 (25.5)	-	-	11.3 (8.8)	-	-	1.8 (1.3)
PTA/SSA	33.7	-	-	-	3.1	0.9	8.5	52.3	1.5	9.4	0.16	-	2.7
SWN ^{b)}	44.6 (50.1)	- (2.3)	1.6 (2.6)	-	16.1 (16.9)	-	35.4 (29.3)	-	-	-	-	-	2.2 (1.8)
PTA/SWN ^{b)}	28.6	-	-	-	3.2	-	9.3	57.9	1.0	-	0.16	-	2.9
TSM	37.5 (39.9)	-	4.2 (7.5)	14.4 (9.5)	15.3 (15.1)	-	28.7 (28.0)	-	-	-	-	2.0 (2.9)	1.9 (1.9)
PTA/TSM	20.5	-	-	1.9	2.8	-	5.7	69.1	-	-	0.08	3.0	2.0
SME	36.7 (40.6)	-	2.8 (5.0)	11.4 (9.4)	15.1 (16.5)	0.2 (0.14)	31.1 (28.3)	-	-	-	-	2.7 (3.0)	2.1 (1.7)
PTA/SME	25.6	-	-	3.9	6.7	0.4	15.8	47.2	0.3	-	0.33	4.1	2.4
PTA	18.8 (22.2)	-	-	-	-	-	-	79.6 (76.6)	1.6 (1.1)	-	-	-	-

^a S element is present as an impurity in SSA (see reference: Vuillaume et al., 2009); ^{b)} a correction has been used to consider the undetected amount of Lithium (% Li = 2.3).

Powder X-ray diffraction (XRD) allows for the measurement of the basal spacing (repeat period) in the out-of-plane direction of the clay. This distance includes the tetrahedral and octahedral layer sheets as well as the gallery interlayer gallery where the counter-ion are confined in the solid state (see scheme 1). The diffraction patterns of all the products obtained at ambient temperature are presented in Figure 4 and the associated data are given in Table 2. For the two smectite clays, SSA and SWN, the low-angle region of the diffractograms (Figure 4. a,b) shows a broad Bragg peak at $\sim 7.5^\circ$ which results from the limited but regular stacking of the silicate plates. For SSA, the calculated basal spacing is 11.7 Å while for SWN an accurate determination of the basal spacing is barely possible due to the ill-defined shape of the peak. With this limitation in mind, we decided to resort to an analysis of the Patterson functions, P(r), which have shown to be appropriate to investigate disordered systems (Vuillaume et al., 2003; Arys et al., 2003). P(r) functions allow for an analysis in the real space rather than in the reciprocal space. The presence of translational ordering is indicated by regularly spaced oscillations and the distance between two oscillations may help to determine the basal spacing of the clays. P(r) functions were computed from the X-ray transmission experiments (see experimental part) and representative P(r) traces are shown in the right part of the Figure 4. Data resulting from the analysis of the Patterson functions are given in the Table 2. For SSA, the basal spacing (11.4 Å) determined from the position of the first oscillations (see Figure 4. h) coincides well with the value calculated from the (001) Bragg reflection (see Table 2) and with literature data (Peeterbroeck et al., 2005).

For SWN, the basal spacing obtained from P(r) function was 11.6 Å (Table 2 and Figure 4. f) which is slightly shorter than data reported elsewhere (Utracki et al., 2006). Repeat period is generally calculated from the consecutive distance between the successive oscillations but for the two smectite clays, oscillations are irregularly spaced, reflecting their poorly organized character. In this connection, the exponential damping of the Patterson functions allows for the determination of the extent of the coherent out-of-plane stacking. For SSA and SWN, the size of the ordered regions (or correlation lengths) was respectively 24 and 27 Å.

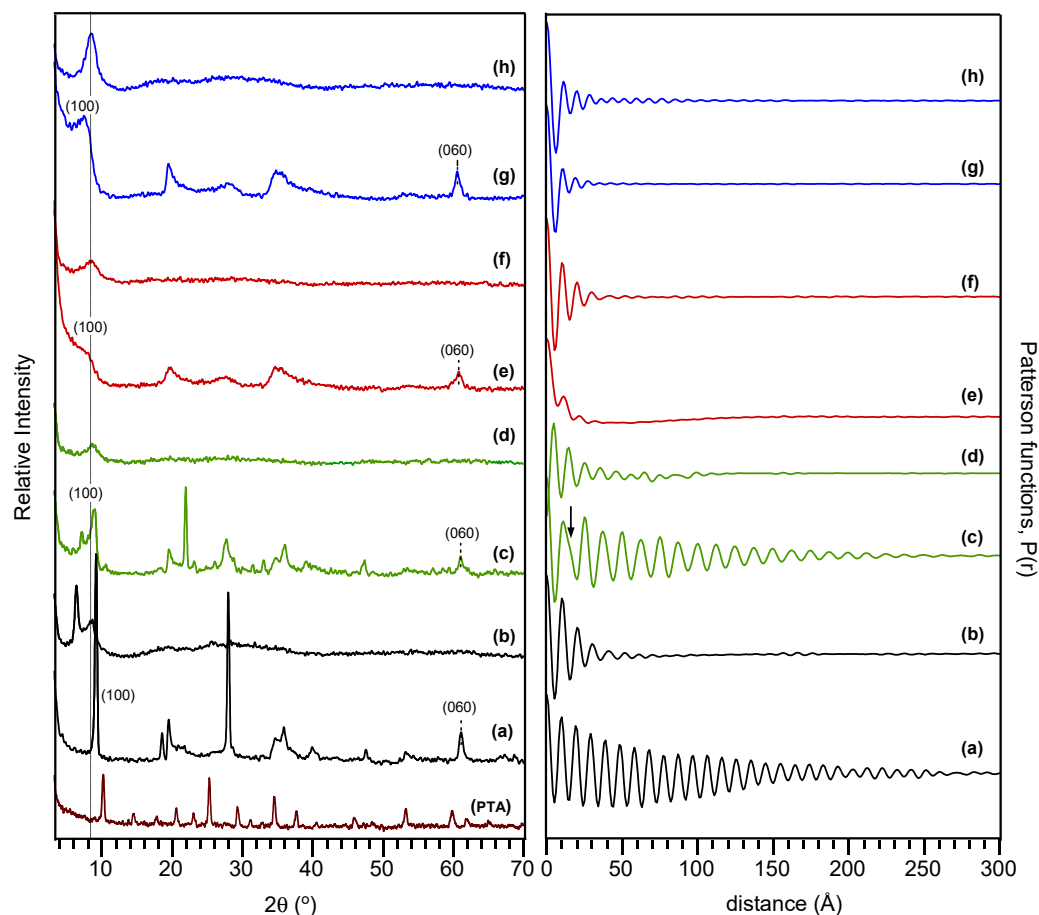


Figure 4. Left: X-ray reflectograms of PTA heteropolyacid, clays and PTA-clay complexes prepared at a weight ratio of 5: PTA; a) SME; b) PTA/SME; c) TSM; d) PTA/TSM; e) SWN; f) PTA/SWN; g) SSA; h) PTA/SSA.

Data are displaced vertically for clarity and lines are a guide for the eyes and help to indicate the invariant position of the Bragg reflection observed for the complexes. Right: Patterson functions of clays and PTA-clay complexes (prepared at a weight ratio of 5 and exposed to room atmosphere) computed from the X-ray transmission experiments: a) SME; b) PTA/SME; c) TSM; d) PTA/TSM; e) SWN; f) PTA/SWN; g) SSA; h) PTA/SSA. Data are displaced vertically for clarity. Arrow indicates the interdistance at which is seen the additional periodic function (see text for details)

Table 2. Structural data of clays and complexes (formed at a PTA-clay weight ratio of 5) obtained from the X-ray reflection data and computed from Patterson functions obtained from the X-ray transmission experiments

	SSA	PTA/SSA	SWN	PTA/SWN	TSM	PTA/TSM	SME	PTA/SME
2θ ($^{\circ}$)	7.54	8.46	^{h)}	8.35	7.16;8.90 ^{e)}	8.64	9.16	6.38;8.48 ^{e)}
δ_B (\oplus) ^{a)}	11.7	10.5	-	10.6	12.4;9.94	10.2	9.65	13.9;10.4
δ_B^1 (\oplus) ^{b)}	11.4	10.7	11.6	10.6	11.0 ^{d)}	10.1	9.8	10.5
$\Delta\delta$ (\oplus) ^{c)}	^{g)}	^{g)}	11	10	12	10	10	10
ζ (\oplus)	8	9	9	14	60	21	75	19
Λ_X (\oplus) ^{d)}	24	27	27	42	180	63	225	57

^{a)} Bragg spacings calculated from the first (001) reflections; ^{b)} Bragg spacings obtained from the maximum of the first oscillation of the Patterson function; ^{c)} Bragg spacings obtained from subsequent and regularly spaced oscillations detected in Patterson functions; ^{d)} coherence length; ^{e)} superposition of two Bragg peaks (see text for details); ^{f)} a shoulder is present on the first oscillation of the Patterson function (see text for details); ^{g)} no regularly spaced significant oscillations detected in Patterson functions; ^{h)} Bragg reflection is too broad for an accurate measurement of the Bragg spacing.

In addition to the occurrence of the Bragg peaks observed in the small angle region of the reflectograms, SSA and SWN are characterized by a similar profile at larger angles, with broad Bragg peaks reflecting the low degree of in-plane order (crystallinity) existing within the layers. For both smectite clays, the occurrence of trioctahedral layered materials is suggested by the value of 1.52 Å calculated from the (060) reflection peak.

Mica clays reflectograms contrast markedly with those of the smectite clays. In the low angle region, TSM and SME can present one or two Bragg peaks depending on the drying conditions. For TSM, the calculated d-spacings are 9.94 and 12.4 Å. The former is the characteristic value obtained for non-hydrated mica (Okada, Morita & Ogawa, 2005) and reflect the interlayer spacing without intercalated water while the latter corresponds to basal spacing retaining water molecules (hydration of the intercalated ions) under ambient conditions. This coexistence of two kinds of interlayers was reported for other for mica-type clays (Tateyama et al., 1998; Yang, Han, Choy, & Tateyama, 2001; Imai et al., 2002; Inoue et al., 2001; Hata, Kobayashi, & Mallouk, 2007). The shoulder found on the first oscillation of the Patterson function at weak interdistance (< 30 Å) indicates the superposition of two different periodic functions (Figure 4. c) which reflect the two types of basal spacing discussed above. For mica clays, Bragg peaks related to the basal spacing are much narrower than for smectite clays and, for SME, the second and third order reflection peaks are also visible. The associated P(r) functions shows that ordered regions (or correlation lengths) corresponding to longitudinal packing of the platelets extends over much larger distances than for smectites (Table 2), namely on a length scale of at least 180 Å for mica. In the wide-angle region, the two mica profiles present similar features. The sharpness and intensity of the Bragg reflections indicates higher in-plane correlation length than for the smectite clays as well as a higher degree of crystallinity.

For PTA, the large number of reflections seen in the diffractogram obtained at room temperature reflects its crystalline nature (Figure 4). The PTA acidic treatment changes markedly the profiles of the clays, particularly in the wide-angle region where (hkl) Bragg reflections are replaced by broad halos between 20 and 40° (Figure 4). This along with the complete vanishing of the (060) reflection peak indicates the quasi-total loss of the in-plane ordering (tetrahedral and octahedral sheets) and therefore, the destruction of a large part of both smectite- and mica-type structures. It is worthy to note that, for the mica complexes, a magnification of the profiles in the wide-angle region (12-40°) reveal the presence of barely visible reflections (see Figure 4) indicating that a weak proportion of the clay has preserved its crystalline structure. For all complexes, no peaks related to the presence of PTA can be observed. This is only possible if PTA acid is incorporated as a poorly ordered crystalline phase or under the form of small crystallites size. These elements suggest, in agreement with the literature, the occurrence of a dominating amorphous silica phase, as corroborated by DRIFT experiments (see below), in which PTA is self-assembled at the nanoscale level (Okada et al., 2006).

Besides the disruption of the in-plane order indicating the loss of substantial crystallinity, low-angle region of the PTA-clay profiles present at least one Bragg peak which indicates, similarly to data reported previously (Temujin, Okada, & MacKenzie, 2003) that some kind of order is retained despite the harsh acidic PTA treatment. It is striking to note that all PTA-clay complexes are characterized by a broad quasi-invariant Bragg peak centered at about 8.5°. The corresponding Bragg spacing (10.4 Å; $S_d = 0.2$ Å) is coincident with the diameter of the Keggin anion (~10 Å) and to the thickness for a 2:1 silicate layer (9.3 - 9.6 Å). At this step, it is interesting to compare these results with those obtained for polyoxometalate-LDH complexes reported earlier (Yun & Pinnavaia, 1996). This peak of relatively weak intensity is strikingly reminiscent of that observed for pillared systems based on Keggin (Yun & Pinnavaia, 1996; Wang, Tian, Wang, & Clearfield, 1992; Narita, Kaviratna, & Pinnavaia, 1993; Weber et al., 1993). For these systems, a broad reflection is similarly centered at $\sim 2\theta = 8^\circ$ (11 Å) suggesting, if we consider the results of the present work, that the position of the peak is independent of the structure (in particular the thickness) the layered structure [layers thickness of 2:1 phyllosilicate is twice that of LDH (4.8 Å)]. However, the repeat distance depends on the structure of the heteropolyacids (Yun & Pinnavaia, 1996). Several hypotheses have been discussed by Pinnavaia and coworkers for explaining the presence of this peak (Yun & Pinnavaia, 1996). The formation of some uncommon pillared phase or hydrolyzed POM was first ruled out (due to the symmetry of the Keggin structure and from FTIR experiments, respectively) and they rather tentatively ascribed the presence of the peak to the formation of some quasi-crystalline POM salt formed during the pillaring reaction (Yun & Pinnavaia, 1996).

On the other hand, we reported in a previous publication that, for PTA-SSA complexes formed at lower weight ratios (2 and 3) (lower content of W element), the intensity of this reflection tended to be much more intense and the repeat spacing slightly larger. On the other hand, for complexes obtained from smectite and mica clays, the coherence length obtained from the Patterson functions (Table 2) indicate that complexes are still partially ordered. PTA-SWN complexes are characterized by ordered regions that slightly extended in size ($L_c = 42$ Å) compared to the virgin clay ($L_c = 27$ Å, stacking of the clay). In contrast, for mica-based complexes, coherence lengths are

dramatically decreased from 180 to approximately 60 Å but remains slightly higher than that of the smectite clays. The preservation of the structural integrity of the stacking can be speculatively explained by the hydrophobic behaviour of the mica clay to the presence of fluorine elements covalently attached to the structure.

Complex based on SWN is different from the others due to the presence of a second Bragg reflection found at lower angle ($2\theta = 6.3^\circ$; 13.9 Å). This could reflect the formation of intercalation compounds containing divalent counterions formed from the depleted Mg^{2+} ions emanating from the octahedral layers.

The SEM images of the clays and their complexes illustrated in Figure 5 were obtained according to a procedure involving a short sonication time in methanol (see the experimental part). Obviously, it is expected that such conditions activate some decomplexation process resulting in substantial PTA release (which was in fact verified by EDX spectroscopy). However, such treatment may also leave behind a significant number of particles with different degree of clustering, allowing for detailed observations of morphology and surface texture. For the two smectite clays, SSA and SWN, images presented in Figure 5. a,c shows some stacking of exfoliated silica sheets with size significantly less than one micron and typically in the range from 100 to 500 nm. Topographic observations of SWN (Figure 5. c) also reveal aggregates with very small sizes (< 200 nm) with round forms and sometimes spherical aggregates.

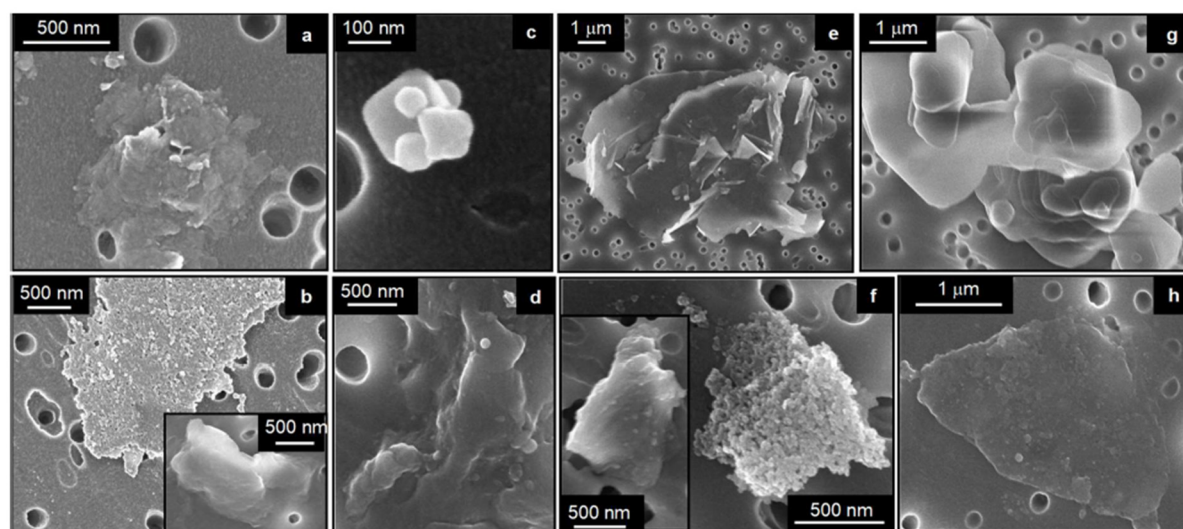


Figure 5. Representative SEM images of samples showing the morphology of neat clays and PTA-clay complexes prepared at a weight ratio of 5: a) SSA; b) PTA-SSA; c) SWN; d) PTA-SWN; e) TSM; f) PTA-TSM; g) SME; h) PTA-SME. Insets of b) and f) images present other views of the complexes at the same magnification but in another location

Aggregates were also evidenced from micrographs of (fluoro)mica clays but sizes are in the submicron-micron range ($> 5 \mu\text{m}$). All virgin clays aggregates present a smooth surface, sometimes crumpled for TSM (Figure 5. e) and with round shape for SME. This generally contrasts with the rough and irregular surface texture observed for the PTA-clay complexes (Figure 5. b,f). The aggressive PTA attack of the surface clay is particularly visible in all the complex images (see Figure 5. b,f) by the occurrence of a well-developed porous-like surface. Even, after PTA treatment of the clay and the impact of sonication in methanol, images suggest that there is still the production of materials with layered morphology (Figure 5. b(inset),f,h) but with variable and irregular surface textures.

To complement the XRD experiments observations, Fourier transformed diffuse reflectance spectroscopy (DRIFT) studies were undertaken (see Figure 6). As demonstrated elsewhere for smectite clay (Vuillaume et al., 1998), DRIFT is very sensitive to structural modifications of the clay when activated with PTA (Linssen et al., 2002; Okada, Morita, & Ogawa, 2005). Between 1400 and 400 cm^{-1} , bands characteristic to Si-O bonds in the tetrahedral sheet, and also to Mg-O stretching vibrational bonds are identified. This region also provides the main vibrations bands characteristic of the PTA Keggin structure. Figure 6 presents the DRIFT spectra of PTA acid, pristine clays and PTA-clay complexes formed at a PTA-clay weight ratio of 5. SSA DRIFT spectrum was detailed elsewhere but the main features can be briefly reported (Vuillaume et al., 2009).

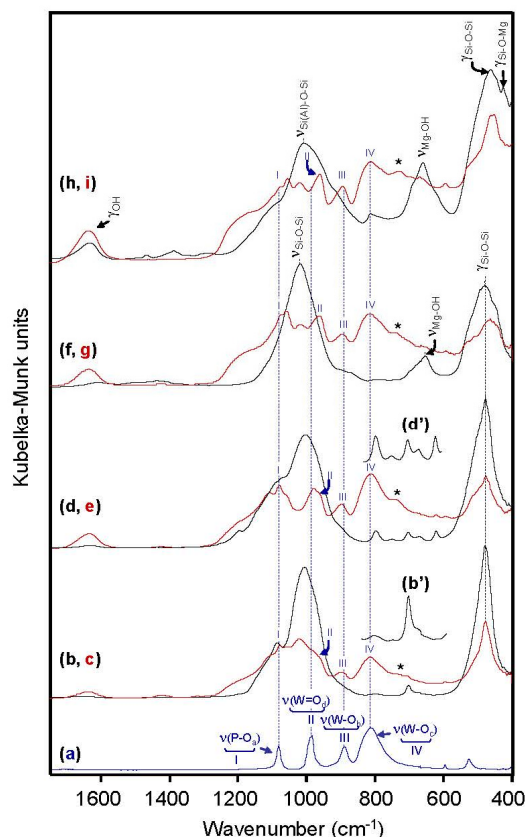


Figure 6. DRIFT spectra measured for dried PTA, pristine clays [as a powder, non exfoliated] and their complexes with PTA: a) PTA; b, b') SWN; c) PTA/SWN; d, d') TSM; e) PTA/TSM; f) SME; g) PTA/SME; h) SSA; i) PTA/SSA. Peak I, II, III IV are the vibration bands corresponding to the Keggin structure of PTA. The blue vertical dotted lines indicate the position of the PTA Keggin vibration bands. b') and d') spectra are magnifications of the 850-600 cm^{-1} region of SME and TSM mica-type clays

The three major sets of vibrations bands that characterised the tetrahedral sheet of silicate are found at ~ 1006 , 659 and 462 cm^{-1} (Figure 6. h) (Farmer, 1974). The broad and intense band observed at 1006 cm^{-1} is assigned to Si(Al)-O-Si stretching vibration mode ($\nu_{\parallel}\text{Si(Al)-O}$) while the two others at 659 and 462 cm^{-1} can be ascribed to Mg-OH stretching ($\nu_{\text{Mg-O}}$, octahedral sheet) and Si-O-Mg bending ($\gamma_{\parallel}\text{Si-O}$) vibrations, respectively. The shoulder observed at 693 cm^{-1} is assigned to Al-OH vibration band in the octahedral sheet. For the hectorite-type clay, SWN, the set of vibration bands described above can be found at 1019 , 656 , and 480 cm^{-1} (Figure 6. f). The less intense band found at $\sim 800 \text{ cm}^{-1}$ and the shoulder at $\sim 701 \text{ cm}^{-1}$ are believed to be related to Si-O out of plane bending vibration ($\nu_{\perp}\text{Si-O}$) (Vicente et al., 1996; Farmer, 1958) SWN spectrum (Figure 6. f) also contains a band at 654 cm^{-1} that can be attributed to OH bending (Farmer, 1968). In the Si-O bending mode region ($400\text{-}600 \text{ cm}^{-1}$), the observed complex band contains more than one vibrational contribution. Nevertheless, although the whole assignment bands are still uncertain, those seen at 532 and 443 cm^{-1} can be attributed to $\gamma_{\parallel}\text{Mg-O}$ and $\nu_{\perp}\text{Mg-O}$ or $\gamma_{\parallel}\text{Si-O-Al}$, respectively (Li, Liu, Ge, Xu, Rocha & Klinowski, 1993). Mica clays, TSM and SME, present a similar DRIFT spectrum in the $1400\text{-}400 \text{ cm}^{-1}$ region (Figure 6. b,d). The tetrahedral Si-O bands are observed at 1086 ($\nu_{\perp}\text{Si-O}$), 1006 ($\nu_{\parallel}\text{Si-O}$), and 480 cm^{-1} ($\gamma_{\parallel}\text{Si-O}$) for SME and 1195 , ~ 1077 ($\nu_{\perp}\text{Si-O}$), 1004 ($\nu_{\parallel}\text{Si-O}$) and 478 ($\gamma_{\parallel}\text{Si-O}$), cm^{-1} for TSM. The tetrahedral Si-O bands are observed at 1086 ($\nu_{\perp}\text{Si-O}$), 1006 ($\nu_{\parallel}\text{Si-O}$), and 480 cm^{-1} ($\gamma_{\parallel}\text{Si-O}$) for SME and 1195 , ~ 1077 ($\nu_{\perp}\text{Si-O}$), 1004 ($\nu_{\parallel}\text{Si-O}$) and 478 ($\gamma_{\parallel}\text{Si-O}$), cm^{-1} for TSM. For both mica clays, a set of less intense typical mica-type clays vibration bands is observed in the $850\text{-}600 \text{ cm}^{-1}$. For TSM complex, the assignment of this mode is uncertain due to the contribution of two vibrational modes. This feature is consistently accompanied in all spectra - although less distinctively for the mica-type based complexes - by the apparition of broad shoulder, near 1200 cm^{-1} . Also, subtraction of the pristine clay spectrum from that of the complexes (see Figure 7) also helps to reveal the position of other new vibrations bands at 1060 and $470\text{-}450 \text{ cm}^{-1}$ which are putatively assigned to Si-O vibrations of amorphous silica with a three-dimensional framework originated during

acid treatment (Moenke, 1974). Additional vibration bands likely related to the occurrence of an amorphous lattice and resulting from the thermal treatment of the complexes will be discussed below.

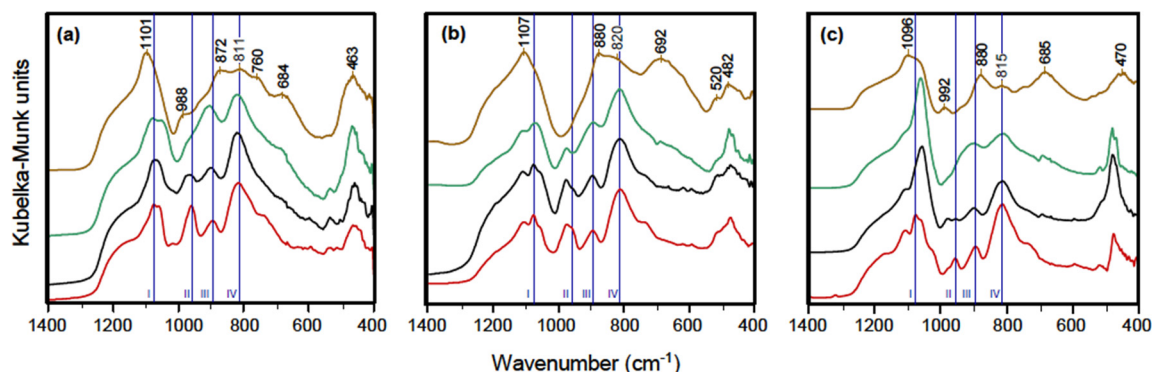


Figure 7. DRIFT difference spectra PTA-clay complexes prepared at a weight ratio of 5 (subtracted from the spectrum of the clay measured at the same temperature) in the 1400-400 cm^{-1} region. a) PTA/SWN; b) PTA/TSM; c) PTA/SME heated at different temperatures under dynamic vacuum (unless otherwise mentioned): 110 $^{\circ}\text{C}$, red; 280 $^{\circ}\text{C}$, dark; 450 $^{\circ}\text{C}$, green (static vacuum); 650 $^{\circ}\text{C}$, brown (under air atmosphere). Spectra were scaled to the same intensity for a comparison. For Sumecton SA (SSA), changes in the spectra as a function of temperature were found very similar to those observed for SWN (see ref.: Vuillaume et al., 2009). I, II, III and IV are the vibration modes corresponding to the Keggin structure of PTA, namely P-O_a-W, W=O_d, W-O_b-W and W-O_c-W, respectively. Blue dotted lines indicate the position attributed to the Keggin bands in the complexes. Wavenumbers are given for the new vibration modes observed for the complexes heated at 650 $^{\circ}\text{C}$

For complexes based on smectite clays, SSA and SWN, the Mg-OH vibration band found at 656 cm^{-1} is markedly decreases in intensity due to the PTA treatment and is consistent with EDX data indicating the depletion of Mg cations from the octahedral layers.

The spectrum of pure PTA (Figure 4. a) is characterized by four major bands in the 1200-700 cm^{-1} region which are characteristic of its Keggin structure. These are observed at 1081, 986, 892 and 812 cm^{-1} and are associated to P-O_a-W, W=O_d, W-O_b-W and W-O_c-W vibrations mode, respectively. For all the complexes dried at 110 $^{\circ}\text{C}$, the Keggin vibration bands are clearly evidenced in Figure 7. c,e,g,i. As noted elsewhere for SSA-PTA complexes (Vuillaume et al., 2009), the position of the P-O_a-W band for all of the complexes was found at 1077-1079 cm^{-1} , namely relatively close from that of pure PTA (1081 cm^{-1}). Previous reported experiments based on SSA-PTA complexes also revealed that the position of the corner-shared (W-O_b-W) and edge-shared (W-O_c-W) vibrations did not vary significantly. For example, when PTA was complexed to SSA at a weight ratio of 5, both W-O_b-W and W-O_c-W mode only shifts by 1 cm^{-1} . In this work, similar observations have been done for SME and TSM mica complexes. More interestingly, these results contrast with the pronounced red shift (26 and 23 cm^{-1}) of the pure stretching W=O_d vibration band observed for SSA and SWN complexes, respectively. For the mica complexes, the assignment is less straightforward since the band contain more than one vibration contribution probably resulting from the splitting of the W=O_d vibration band as reported elsewhere (Rocchiccioli-Deltcheff et al., 1983).

The Figure 7 presents the spectra of the complexes subtracted from the clay spectra as a function of the heating treatment. The subtracted spectrum of the SME complex confirms the presence of the W=O_d vibration band at 955 cm^{-1} (Figure 7.c), revealing a remarkable red shift by ~ 30 cm^{-1} . For TSM complex, this band is assumed to be centered at 957 cm^{-1} rather than 971 cm^{-1} , shifting similarly by 29 cm^{-1} . Rocchiccioli-Deltcheff and co-workers demonstrated for various polyoxometalates that the decrease in the W=O_d mode frequency correlates well with the size of the counterions, lower stretching frequencies resulting from larger counterions (Rocchiccioli-Deltcheff et al., 1983). (Note 2) In the present case, the large size of clays platelets is probably enough to keep the counterions far apart, limiting considerably the strong repulsive anion-anion interaction (Note 3) and probably precluding any PTA crystallization within the complexes as suggested above by XRD. We decided to examine the effect of the temperature on the DRIFT spectra of the complexes as it should provide information into the type of interaction between clay and PTA and the thermal stability of the complex. DRIFT spectra obtained after heating clays and

complexes at various temperatures are presented in Figure 7. As also noted for SSA elsewhere, heating SSA-PTA complex at 280 °C does not produce major changes in the region 1400–400 cm^{-1} region. As demonstrated in several studies. W-O vibration modes are sensitive to changing electrostatic and to H-bonding interactions. In the present work, among the four major vibration modes related to PTA, $\text{W}=\text{O}_d$ still appears the key one to monitor the complexation between PTA and the clay. For SWN complex, the $\text{W}=\text{O}_d$ band is moderately broadened at 280 °C. However, when heated at 450 °C, the latter is markedly reduced in intensity and shifted from 961 to 977 cm^{-1} . This can be attributed to the weakening of PTA-clay interactions. As reported for SSA, all other bands related to the Keggin structure are still observed indicating that the cage-like structure of PTA is preserved. In contrast, SME complex is much more sensitive to temperature than the other PTA-clay complexes. At 280 °C, $\text{W}=\text{O}_d$ vibration mode tend to be significantly blue shifted, but a less intense vibration is still centered at its initial position, indicating that a significant amount still strongly interacts with the clay. Concomitantly, the $\text{P}-\text{O}_a-\text{W}$ vibration mode appears absent from the spectrum. This also contrasts with the observations of the other mica based (TSM) complex, which appears very robust up to 450 °C, as indicated by the presence of all associated Keggin bands. The higher thermal stability of TSM vs SME micas cannot be clearly explained but could result from the presence of pure SiO_2 tetrahedral sheets while for SME, few Al^{3+} ions replaced Si^{4+} ions, creating, in addition, negatively charged tetrahedral layers. It is thus interesting to note that even a relatively high increase in temperature may not allow for the vibration to reach its “original position”, i.e., that observed for the pristine clays. This suggests that strong attractive interactions between complementary charges also prevail between PTA and clay, in particular for TSM.

With temperature, $\text{W}-\text{O}_b$ and to a less extent $\text{W}-\text{O}_c$ spectral vibrations are modulated in their position by the type of clays used as support. For instance, when heated at 450 °C, the two abovementioned vibrations of the complex based on Lucentite clay (Figure 7. a) were shifted indicating some geometrical distortions of the Keggin structure. In contrast, mica clays appear more robust in helping the preservation of the Keggin structure (Figure 7. b-c).

Also, as mentioned above, new vibrations were noticed after PTA treatment. Temperature is also an element promoting the apparition of new peaks that are clearly evidenced after the subtraction of the clay spectrum (see Figure 7 a-c). Unambiguously, after heating complexes at 650 °C, none of the bands attributed to the Keggin structure cannot be no longer observed. This is in agreement with the structural transition observed by DTA for PTA and PTA/SSA complexes elsewhere (Vuillaume et al, 2009). The other broad bands mentioned above were observed at ~ 1100 , 880, 680 and 460–480 cm^{-1} which were found at nearly the same positions than to the tectosilicates either, 950–1200; 400–550 and 550–850 cm^{-1} (Moenke, 1974). (Note 4)

4. Conclusions

Various protogenic inorganic complexes were obtained by self-assembling 12-phosphotungstic acid with synthetic smectite and (fluoro)mica phyllosilicates clays. Thermal, morphological, and structural properties were studied by FTIR, SEM and XRD. The aggressive PTA attack of the surface clay is evidenced in all complex images obtained by SEM. According to the Patterson functions, coherence lengths - which reflect the longitudinal platelet stacking are, for the virgin clays, significantly lower for the two smectite clays ($L_c \sim 25 \text{ \AA}$) than for their analogous of the mica type ($L_c = 180\text{--}225 \text{ \AA}$). After PTA acid treatment, all the phyllosilicate-clay complexes which are characterized by a clear amorphous-like character, maintain a stratified local order which do not extend over a distance larger than 60 \AA . This lamellar-like organization agrees with the observations obtained from SEM images. The solid-state organization of the complexes is reminiscent of smectic cybotactic liquid crystalline phases i.e. whose coherence length is limited on only few layers. On the other hand, PTA-clay complexes present a good thermal stability from room temperature up to 280 °C. Even at 450 °C, The Keggin structure within the complexes seems preserved especially for TSM mica clays. However, at temperatures above 450 °C, the cage-like structure is elusive, and a substantial proportion of tectosilicate-like materials is generated due to the degradation of the clays.

Acknowledgments

The financial support of the NRC Fuel Cell and Hydrogen Program is gratefully acknowledged. The authors would like thank K. Théberge (CNRC, IMI) for XRD and SEM measurements. We are thankful to N. Côté and D. Desgagné (CNRC, IMI) for their technical contribution to the DRIFT experiments. F. Perrin (CNRC, IMI) is also acknowledged for the SEM contribution. A special thank you to C. Jacques (COALIA) is extended here for its contribution to ensure the general presentation of the document.

Conflict of Interests

The authors declare that there are no conflicts to declare.

Acknowledgments

The financial support of the NRC Fuel Cell and Hydrogen Program is gratefully acknowledged. The authors would like to thank K. Th  berge (CNRC, IMI) for XRD and SEM measurements. We are thankful to N. Cot   and D. Desgagn   (CNRC, IMI) for their technical contribution to the DRIFT experiments. F. Perrin (CNRC, IMI) is also acknowledged for the SEM contribution. A special thank you to C. Jacques (COALIA) is extended here for its contribution to ensure the general presentation of the document.

References

- Arys, X., Fischer, P., Jonas, A. M., Koetse, M. M., Laschewsky, A., Legras, R., & Wischerhoff, E. (2003). Ordered polyelectrolyte multilayers. Rules governing layering in organic binary multilayers. *Journal of the American Chemical Society*, *125*(7), 1859-1865. <https://doi.org/10.1021/ja0283807>
- Biel  nski, A., & Luba  nska, A. (2004). FTIR investigation on Wells–Dawson and Keggin type heteropolyacids: dehydration and ethanol sorption. *Journal of Molecular Catalysis A: Chemical*, *224*(1-2), 179-187.
- Changwen, H. U., Danfeng, L., Yihang, G., & Enbo, W. (2001). Supermolecular layered double hydroxides. *Chinese Science Bulletin*, *46*, 1061-1066. <https://doi.org/10.1007/BF02900678>
- Farmer, V. C. (1958). The infra-red spectra of talc, saponite, and hectorite. *Mineral Mag.*, *31*, 829-845, <https://doi.org/10.1180/minmag.1958.031.241.03>
- Farmer, V. C. (1968). Infrared spectroscopy in clay mineral studies. *Clay Min.*, *7*, 373-387, <https://doi.org/10.1180/claymin.1968.007.4.01>
- Farmer, V. C. (1974). The IR spectra of minerals. *Mineralogical Society, London, UK*. <https://doi.org/10.1180/mono-4>
- Hata, H., Kobayashi, Y., & Mallouk, T. E. (2007). Encapsulation of anionic dye molecules by a swelling fluoromica through intercalation of cationic polyelectrolytes. *Chemistry of materials*, *19*(1), 79-87. <https://doi.org/10.1021/cm061908c>
- Herring, A. M. (2006). Inorganic–polymer composite membranes for proton exchange membrane fuel cells. *Journal of Macromolecular Science, Part C: Polymer Reviews*, *46*(3), 245-296. <https://doi.org/10.1080/00222340600796322>
- Imai, Y., Nishimura, S., Abe, E., Tateyama, H., Abiko, A., Yamaguchi, A., ... & Taguchi, H. (2002). High-modulus poly (ethylene terephthalate)/expandable fluorine mica nanocomposites with a novel reactive compatibilizer. *Chemistry of Materials*, *14*(2), 477-479. <https://doi.org/10.1021/cm010408a>
- Inoue, K., Tateyama, H., Noma, H., & Nishimura, S. (2001). Estimation of the Structure of an Anhydrous 2: 1-Na Layer Silicate Synthesized from Talc by Intercalation Procedure. *Clay science*, *11*(4), 391-404. <https://doi.org/10.11362/jcssjclayscience1960.11.391>
- Kooli, F., & Jones, W. (1997). Characterization and catalytic properties of a saponite clay modified by acid activation. *Clay Minerals*, *32*(4), 633-643. <https://doi.org/10.1180/claymin.1997.032.4.13>
- Li, L. S., Liu, X. S., Ge, Y., Xu, R., Rocha, J., & Klinowski, J. (1993). Structural studies of pillared saponite. *J. Phys. Chem.*, *97*, 10389-10393. <https://doi.org/10.1021/j100142a021>
- Linssen, T., Cool, P., Baroudi, M., Cassiers, K., Vansant, E. F., Lebedev, O., & Van Landuyt, J. (2002). Leached natural saponite as the silicate source in the synthesis of aluminosilicate hexagonal mesoporous materials. *The Journal of Physical Chemistry B*, *106*(17), 4470-4476. <https://doi.org/10.1021/jp015578p>
- Liu, P. (2007). Polymer modified clay minerals: A review. *Applied Clay Science*, *38*(1-2), 64-76. <https://doi.org/10.1016/j.clay.2007.01.004>
- Madejov  , J., Bujd  k, J., Janek, M., & Komadel, P. (1998). Comparative FT-IR study of structural modifications during acid treatment of dioctahedral smectites and hectorite. *Spectrochimica acta part a: molecular and biomolecular spectroscopy*, *54*(10), 1397-1406. [https://doi.org/10.1016/S1386-1425\(98\)00040-7](https://doi.org/10.1016/S1386-1425(98)00040-7)
- Marme, F., Coudurier, G., & V  drine, J. C. (1998). Acid-type catalytic properties of heteropolyacid H3PW12O40 supported on various porous silica-based materials. *Microporous and mesoporous materials*, *22*(1-3), 151-163. [https://doi.org/10.1016/S1387-1811\(98\)00089-4](https://doi.org/10.1016/S1387-1811(98)00089-4)
- Moenke, H. H. W. (1974) In V. C. Farmer (Ed.), *Infrared Spectra of Minerals* (p. 365). London, UK: Mineralogical Society.

- Nakamura, O., Kodama, T., Ogino, I., & Miyake, Y. (1979). High-conductivity solid proton conductors: Dodecamolybdophosphoric acid and dodecatungstophosphoric acid crystals. *Chemistry Letters*, 8(1), 17-18. <https://doi.org/10.1246/cl.1979.17>
- Narita, E., Kaviratna, P. D., & Pinnavaia, T. J. (1993). Direct synthesis of a polyoxometallate-pillared layered double hydroxide by coprecipitation. *Journal of the Chemical Society, Chemical Communications*, (1), 60-62. <https://doi.org/10.1039/c39930000060>
- Okada, K., Arimitsu, N., Kameshima, Y., Nakajima, A., & MacKenzie, K. J. (2006). Solid acidity of 2: 1 type clay minerals activated by selective leaching. *Applied Clay Science*, 31(3-4), 185-193. <https://doi.org/10.1016/j.clay.2005.10.014>
- Okada, K., Arimitsu, N., Kameshima, Y., Nakajima, A., & MacKenzie, K. J. (2005). Preparation of porous silica from chlorite by selective acid leaching. *Applied Clay Science*, 30(2), 116-124. <https://doi.org/10.1016/j.clay.2005.04.001>
- Okada, K., Nakazawa, N., Kameshima, Y., Yasumori, A., Temuujin, J., Mackenzie, K. J., & Smith, M. E. (2002). Preparation and porous properties of materials prepared by selective leaching of phlogopite. *Clays and Clay Minerals*, 50(5), 624-632. <https://doi.org/10.1346/000986002320679503>
- Okada, K., Yoshizaki, H., Kameshima, Y., Nakajima, A., & Madhusoodana, C. D. (2007). Synthesis and characterization of mesoporous silica from selectively acid-treated saponite as the precursors. *Journal of colloid and interface science*, 314(1), 176-183. <https://doi.org/10.1016/j.jcis.2007.05.036>
- Okada, T., Morita, T., & Ogawa, M. (2005). Tris (2, 2'-bipyridine) ruthenium (II)-clays as adsorbents for phenol and chlorinated phenols from aqueous solution. *Applied Clay Science*, 29(1), 45-53. <https://doi.org/10.1016/j.clay.2004.09.004>
- Peeterbroeck, S., Alexandre, M., Jérôme, R., & Dubois, P. (2005). Poly (ethylene-co-vinyl acetate)/clay nanocomposites: Effect of clay nature and organic modifiers on morphology, mechanical and thermal properties. *Polymer degradation and stability*, 90(2), 288-294. <https://doi.org/10.1016/j.polymdegradstab.2005.03.023>
- Rocchiccioli-Deltcheff, C., Fournier, M., Franck, R., & Thouvenot, R. (1983). Vibrational investigations of polyoxometalates. 2. Evidence for anion-anion interactions in molybdenum (VI) and tungsten (VI) compounds related to the Keggin structure. *Inorganic Chemistry*, 22(2), 207-216. <https://doi.org/10.1021/ic00144a006>
- Sanchez, C., Julián, B., Belleville, P., & Popall, M. (2005). Applications of hybrid organic-inorganic nanocomposites. *Journal of Materials Chemistry*, 15(35-36), 3559-3592. <https://doi.org/10.1039/b509097k>
- Spirlet, M. R., & Busing, W. R. (1978). Dodecatungstophosphoric acid-21-water by neutron diffraction. *Acta Crystallographica Section B: Structural Crystallography and Crystal Chemistry*, 34(3), 907-910. <https://doi.org/10.1107/S0567740878004306>
- Tateyama, H., Noma, H., Nishimura, S., Adachi, Y., Ooi, M., & Urabe, K. (1998). Interstratification in expandable mica produced by cation-exchange treatment. *Clays and Clay Minerals*, 46, 245-255. <https://doi.org/10.1346/CCMN.1998.0460304>
- Temuujin, J., Okada, K., & MacKenzie, K. J. (2003). Preparation of porous silica from vermiculite by selective leaching. *Applied Clay Science*, 22(4), 187-195. [https://doi.org/10.1016/S0169-1317\(02\)00158-8](https://doi.org/10.1016/S0169-1317(02)00158-8)
- Tran, N. H., Wilson, M. A., Milev, A. S., Dennis, G. R., McCutcheon, A. L., Kannangara, G. S. K., & Lamb, R. N. (2006). Structural-Chemical Evolution within Exfoliated Clays. *Langmuir*, 22(15), 6696-6700. <https://doi.org/10.1021/la060737n>
- Utracki, L. A., Seppehr, M., & Boccaleri, E. (2007). Synthetic, layered nanoparticles for polymeric nanocomposites (PNCs). *Polymers for advanced technologies*, 18(1), 1-37. <https://doi.org/10.1002/pat.852>
- Vicente, M. A., Suárez, M., López-González, J. D. D., & Banares-Munoz, M. A. (1996). Characterization, surface area, and porosity analyses of the solids obtained by acid leaching of a saponite. *Langmuir*, 12(2), 566-572. <https://doi.org/10.1021/la950501b>
- Vuillaume, P. Y., Glinel, K., Jonas, A. M., & Laschewsky, A. (2003). Ordered polyelectrolyte "multilayers". 6. Effect of molecular parameters on the formation of hybrid multilayers based on poly (diallylammonium) salts and exfoliated clay. *Chemistry of materials*, 15(19), 3625-3631. <https://doi.org/10.1021/cm021338q>

- Vuillaume, P. Y., Mokrini, A., Siu, A., Théberge, K., & Robitaille, L. (2009). Heteropolyacid/saponite-like clay complexes and their blends in amphiphilic SEBS. *European polymer journal*, 45(6), 1641-1651. <https://doi.org/10.1016/j.eurpolymj.2009.01.001>
- Wang, J., Tian, Y., Wang, R. C., & Clearfield, A. (1992). Pillaring of layered double hydroxides with polyoxometalates in aqueous solution without use of preswelling agents. *Chemistry of materials*, 4(6), 1276-1282. <https://doi.org/10.1021/cm00024a030>
- Weber, R. S., Gallezot, P., Lefebvre, F., & Suib, S. L. (1993). Partial pillaring of layered double hydroxides by [SiW₉V₃O₄₀]⁷⁻. *Microporous Materials*, 1(3), 223-227. [https://doi.org/10.1016/0927-6513\(93\)80081-5](https://doi.org/10.1016/0927-6513(93)80081-5)
- Yadav, G. D. (2005). Synergism of clay and heteropoly acids as nano-catalysts for the development of green processes with potential industrial applications. *Catalysis Surveys from Asia*, 9(2), 117-137. <https://doi.org/10.1007/s10563-005-5997-x>
- Yang, J. H., Han, Y. S., Choy, J. H., & Tateyama, H. (2001). Intercalation of alkylammonium cations into expandable fluorine mica and its application for the evaluation of heterogeneous charge distribution. *Journal of Materials Chemistry*, 11(4), 1305-1312. <https://doi.org/10.1039/b006059n>
- Yun, S. K., & Pinnavaia, T. J. (1996). Layered double hydroxides intercalated by polyoxometalate anions with Keggin (α -H₂W₁₂O₄₀⁶⁻), Dawson (α -P₂W₁₈O₆₂⁶⁻), and Finke (Co₄(H₂O)₂(PW₉O₃₄)₂¹⁰⁻) structures. *Inorganic chemistry*, 35(23), 6853-6860. <https://doi.org/10.1021/ic960287u>

Notes

Note 1. AIPEA Nomenclature Committee Recommendations. *Clay Clay Min.*, 1980, 28, 73-78, <https://doi.org/10.1346/CCMN.1980.0280114>

Note 2. The strong increase in the stretching frequencies was explained by the electrostatic anion-anion interactions resulting from the repulsive negative charge densities beared by the O_d atoms (see Narita, Kaviratna, & Pinnavaia, 1993).

Note 3. A minimal distance of about 6 Å between the O_d atoms of adjacent polyanions seems sufficient to limit anion-anion interactions (see Narita, Kaviratna, & Pinnavaia, 1993).

Note 4. For hectorite, amorphous bands were reported at 1096, 800 and 470 cm⁻¹ (see Vicente, Suarez, Lopez-Gonzalez, & Banares-Munoz, 1996).

Copyrights

Copyright for this article is retained by the author(s), with first publication rights granted to the journal.

This is an open-access article distributed under the terms and conditions of the Creative Commons Attribution license (<http://creativecommons.org/licenses/by/4.0/>).